RAMTRANS
Vol. 11, No. 4, pp. 279–294 (2000)
Nuclear Technology Publishing

SIMULATION OF THE THERMAL BEHAVIOUR OF UF_6 CONTAINMENT PACKAGES IN FIRES

J. C. Ferreri†, A. Clausse‡ and F. Basombrío§*
†Autoridad Regulatoria Nuclear, Av. del Libertador 8250
1429 Buenos Aires, Argentina
‡Comisión Nacional de Energía Atómica and Universidad Nacional del Centro
7000 Tandil, Argentina
§Comisión Nacional de Energía Atómica, 8400 Bariloche, Argentina

Received January 11 2000, amended July 8 2000, accepted July 21 2000

Abstract — Computer simulation results concerning the thermal behaviour of a UF_6 container in fires are presented. The results have been obtained using three different approximations, namely: a coarsely lumped parameter model, a heat conduction model and, finally, a finite element heat conduction model. In all cases, the sinking of the non-melted UF_6 core is not considered. Effective parameters for the heat conduction were used to simulate the heat conduction through the melted material. Accordingly, the effects of the natural convection around the non-melted UF_6 core are not considered. The results are compared with numerical and experimental data in order to assess the performance of the computational approaches.

INTRODUCTION

Uranium hexafluoride (UF_6) is the basic material used to produce enriched uranium for nuclear fuel elements. It is stored and transported in bare cylinders made from steel. Their dimensions are (for 48Y type cylinders): 3.8 m long and 1.22 m internal diameter. They contain 12,500 kg of UF_6. The assessment of the safety of UF_6 transport is an important issue in transport regulations. This is firstly due to the chemical hazard imposed by the hypothetical release of this substance and secondly to its radioactive consequences. Radiological protection literature abounds in detailed considerations of the latter, while only limited attention has been paid to the former. The International Atomic Energy Agency sponsored recent research efforts on the subject through a Coordinated Research Agreement (CRA 7285). This paper summarises the authors' contribution to that project.

An important issue concerning the safety of UF_6 packages is the integrity under external fire conditions. The study of postulated fire accidents involves the analysis of the thermodynamics of UF_6. This material has its triple point at nearly 64°C. When the container is exposed to higher temperatures, the initially solid UF_6 begins to sublimate and liquefy, leaving a remaining solid mass at nearly constant temperature. The melting progresses up to the point at which all the material is liquid, increasing its volume and almost filling all the initially empty space in the container (the 'ullage'). During this process, the container inner pressure increases due to further liquid/vapour expansion and may lead to the failure of the container. The objective of this research is the understanding of the processes dealing with the melting and temperature evolution of the UF_6 during postulated accidents.

On the other hand, the large number of containers existing in stock imposes economic constrains to design changes. Therefore, numerical simulations of the melting process occurring inside the packages provide a useful low-cost tool for the designer.

In this work, the results of computer simulations dealing with the thermodynamic behaviour of UF_6 containers in postulated fires are addressed. The problem is

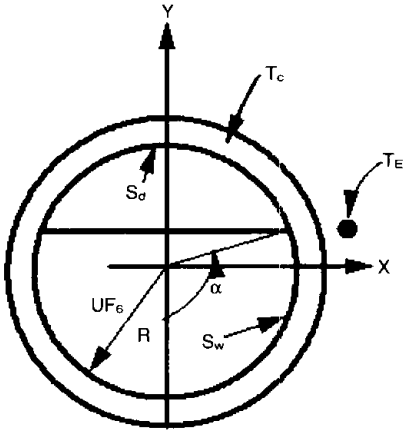

Figure 1. A schematic representation of a cross section of a hypothetical UF_6 container geometry.

* All authors are member of CONILET.
Contact author E-mail: jferreri@cae.arn.gov.ar

tackled at three levels of increasing detail. The different results are compared with previously reported experimental and numerical results showing good agreement.

A SIMPLIFIED LUMPED PARAMETER APPROXIMATION

Let us consider a simplified model of the UF_6 container[1,2]. Figure 1 shows a cross section of a cylindrical steel container of inner radius R_U and wall thickness e. The UF_6 fills a fraction of the total interior area. The fraction of the perimeter that is wetted is denoted by S_w, while the dry fraction is S_d (considering areas). It is justified in the need to consider the finite length of the container. It is important to keep this in mind because the incidence of the wall surfaces at the top and bottom of the cylinder can make a significant contribution to the heat balances, depending on the geometry of the container. The angle α defines the extent of the wetted surface, measured from the lower vertical axis. The heat transfer from the interior container wall to the UF_6 will be limited to the wetted perimeter. Thus, we are considering that the vapour is adiabatic and that radiation from this wall does not contribute to the heat balance. This approximation may hold reasonably up to an interior wall temperature of the order of 400°C.

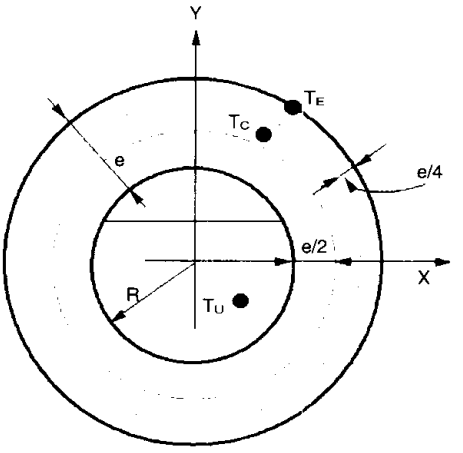

Figure 2. A simple, lumped-parameter representation of the system.

The model assumes that the UF_6 temperature is uniform. The latter is the most restrictive assumption and may be relaxed if the UF_6 is divided in two lumped volumes, one for the liquid and another for the solid. In the sections to follow, this limitation will be eliminated. An additional restricting hypothesis consists in considering that the system internal pressure may be calculated from equilibrium of UF_6 phases. The consequences of this assumption will be discussed later. However, it is worth mentioning here that the equilibrium hypothesis may be limiting, given some experimental evidences[3].

Let us consider the nodalisation of Figure 2, where three temperatures are shown. T_E, represents the steel temperature in a surface node of thickness e/4; T_C, represents the inner steel temperature in a node of thickness 3e/4 and, finally, T_U represents the temperature in the UF_6 (solid or liquid).

The heat balance equations are:

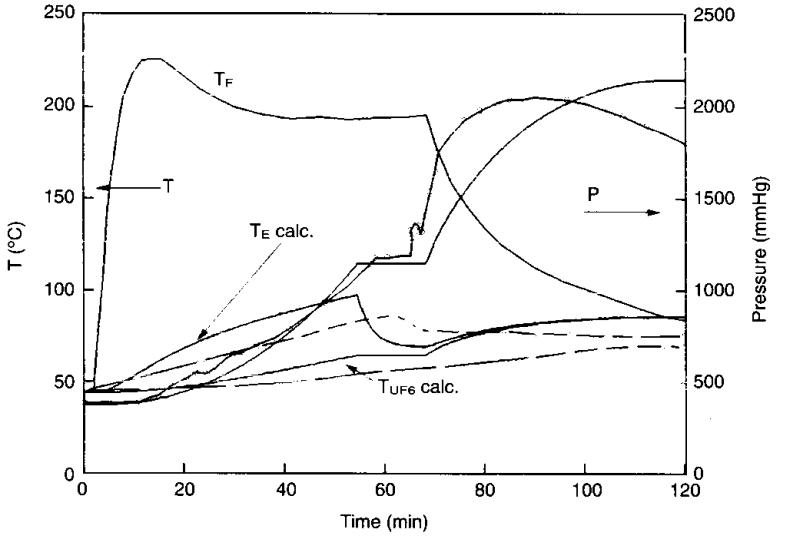

Figure 3. JCRP-10[3] Simulation of Test case 2.4 (200°C). Temperature and pressure evolution. Pressure: (○) exp.[3]; (——) calc.

$$V_U\rho_U C_U \frac{dT_U}{dt} = \frac{S_U}{(R_U/\lambda_U) + (e/2\lambda_C)}(T_C - T_U) \quad (1a)$$

$$V_C^A\rho_C C_C \frac{dT_C}{dt} = \frac{S_U}{(R_U/\lambda_U) + (e/2\lambda_C)}(T_C - T_U) + \frac{S_3}{(e/4\lambda_C)}(T_E - T_C) \quad (1b)$$

$$V_E\rho_C C_C \frac{dT_E}{dt} = -\frac{S_3}{(e/4\lambda_C)} \cdot (T_E - T_C) + H_E S_E(T_F - T_E) \quad (1c)$$

The heat transfer areas are defined based on the radial positions shown in Figure 2. R_U is the effective radius of the UF_6 node. In this approximation, it will be considered coincident with the container inner radius R. T_F is the environment (or 'fire') temperature. In the above expressions, V represents a node volume, M the mass of a given material while C measures its heat capacity and λ its 'effective' conductivity. H_E is the overall heat transfer coefficient between the environment and the steel. This coefficient may include the effects of radiation, via adequate linearisation. The following definitions will be used in the analysis to follow:

$$\tau_U = \frac{M_U C_U}{S_U}\left(\frac{R_U}{\lambda_U} + \frac{e}{2\lambda_C}\right)$$

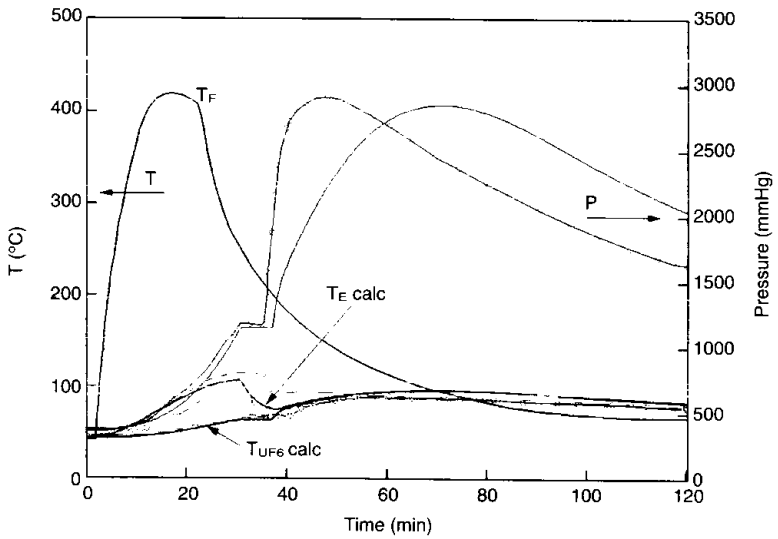

Figure 4. JCRP-10[3] Simulation of Test case 4.1 (400°C). Temperature and pressure evolution. Key as Figure 3. From Reference 3: (–○–) TB2 (steel), (–○–) TB1 (steel), (–▽–) TB3 (UF_6).

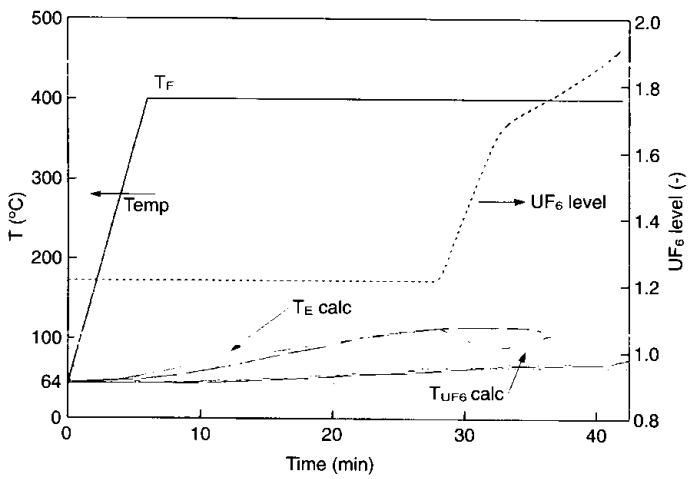

Figure 5. A case with constant fire temperature (T_F = 400°C), geometry as in JCRP-10[3]. UF_6 level evolution.

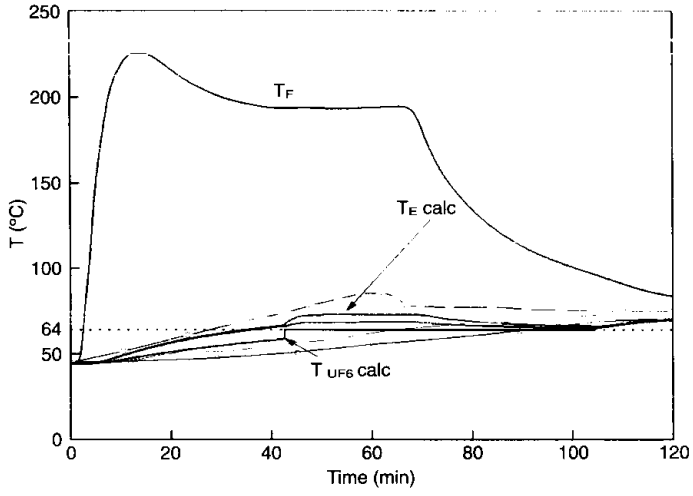

Figure 6. JCRP-10[3] Simulation of Test case 2.4 (200°C) using the heat conduction coupled model. Temperature evolution.

Table 1. Physical data for the simulation[9,10] case 1.

Material	T_{Trip}	C_S	C_L (C_G)	ρ_S	ρ_L (ρ_G)	λ_S	λ_L (λ_G)	H_{FS}
Steel	—	480.0	—	7850	—	43.0	—	—
UF_6	64.0	500.0	558.0	4950	3300	0.9	290.7	$2.77\ 10^8$
Gases	—	—	409.5	—	13.9	—	3.89	—

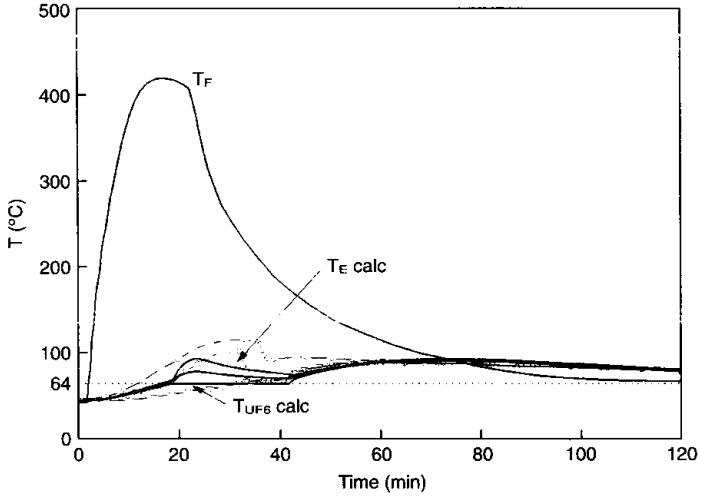

Figure 7. JCRP-10[3] Simulation of Test case 4.1 (400°C) using the heat conduction coupled model. Temperature evolution.

$$\tau_C = A_1 \frac{M_C C_C}{S_U}\left(\frac{R_U}{\lambda_U} + \frac{e}{2\lambda_C}\right)$$

$$\tau_E = \frac{A_1}{B_1}\frac{M_C C_C}{S_U}\left(\frac{e}{4\lambda_C}\right)$$

$$\tau_F = \frac{A_2}{B_2}\frac{M_C C_C}{S_U}\frac{1}{h}$$

$$M_U = \rho_U V_U,\ M_C = \rho_C V_C$$

and

$$A_1 = \frac{V_C^A}{V_C} = \frac{3}{4}\left(\frac{R_U + \frac{3}{8}e}{R_U + \frac{e}{2}}\right)$$

$$A_2 = \frac{V_E}{V_C} = \frac{1}{4}\left(\frac{R_U + e}{R_U + \frac{e}{2}}\right)$$

$$A_3 = \frac{A_2}{A_1}$$

$$B_1 = \frac{S_E}{S_U} = 1 + \frac{e}{R_U}$$

$$B_2 = \frac{S_3}{S_U} = 1 + \frac{3}{4}\frac{e}{4R_U}$$

These definitions are the coefficients to be used in the system of equations describing the variation of temperature in the lumped approximation. They take into account node volumes, surfaces and material properties.

Using the above given definitions, Equations 1(a–c) may be written as:

$$\frac{dT_U}{dt} = \frac{1}{\tau_U}(T_C - T_U) \tag{2a}$$

Table 2. Constants related to thermal radiation BCs, case 1.

σ	ϵ	α
$5.67\ 10^{-8}$	0.8	0.8

Table 3. Some selected points in the container, case 1.

Point	X	Y
C	0.0000	0.6255
D	0.0000	–0.6255
E	0.4474	–0.2901
F	0.3767	–0.2551
G	0.0000	0.0000

$$\frac{dT_C}{dt} = -\frac{1}{\tau_C}(T_C - T_U) + \frac{1}{\tau_E}(T_E - T_C) \tag{2b}$$

$$\frac{dT_E}{dt} = -\frac{1}{A_3\tau_C}(T_E - T_C) + \frac{1}{\tau_F}(T_F - T_E) \tag{2c}$$

This form of the equations puts into evidence the characteristic time scales of the system components. A fully implicit discrete numerical analogue of Equations 2(a–c) will be used. This choice will avoid stability restrictions in the choice of the time step, the only restriction on its value being the solution accuracy.

$$T_U^{n+1} - T_U^n = \alpha\,(T_C^{n+1} - T_U^{n+1}) \tag{3a}$$

$$T_C^{n+1} - T_C^n = -\beta\,(T_C^{n+1} - T_U^{n+1}) + \gamma\,(T_E^{n+1} - T_C^{n+1}) \tag{3b}$$

$$T_E^{n+1} - T_E^n = -\delta\,(T_E^{n+1} - T_C^{n+1}) + \epsilon\,(T_F^{n+1} - T_E^{n+1}) \tag{3c}$$

where

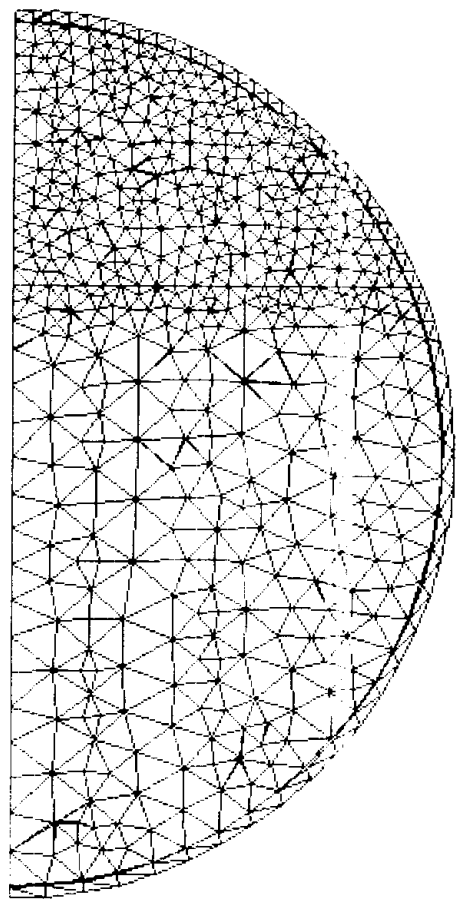

Figure 8. FEM grid used in the simulation of the experiment in Reference 15.

$\alpha = \Delta t/\tau_U$, $\beta = \Delta t/\tau_C$, $\gamma = \Delta t/\tau_E$, $\delta = \Delta t/(A_3\tau_E)$ and $\epsilon = \Delta t/\tau_F$

An even simpler approximation of Equations 2 (a–c) can be obtained assuming that the external wall temperature T_E equals the fire temperature. Then, Equation 1(c) may omitted, and Equation 1(a) and (b) become:

$$\frac{dT_U}{dt} = \frac{1}{\tau_U}(T_C - T_U)$$

$$\frac{dT_C}{dt} = -\frac{1}{\tau_C}(T_C - T_U) + \frac{1}{\tau_E}(T_E - T_C)$$

These equations may be integrated analytically in some particular cases, particularly for constant T_E.

Equations 3(a–c) were solved explicitly for T_U, T_C and T_E as a function of their initial values and the values of $T_E(t)$. Integration proceeds as follows: T_U, T_C and T_E are calculated from Equations 3(a–c) until T_U reaches the value of the triple point temperature (T_{Trip}). From this time up to the moment in which all the UF_6 is melted, its temperature is kept fixed at T_{Trip} and only T_C and T_E are calculated. When all the UF_6 has melted, the solution of Equation 3(a–c) is resumed. The time evolution of the melted fraction of UF_6 is computed from the mass balance, taking into account the variation of the UF_6 density. It is also assumed that all the heat gained from the environment

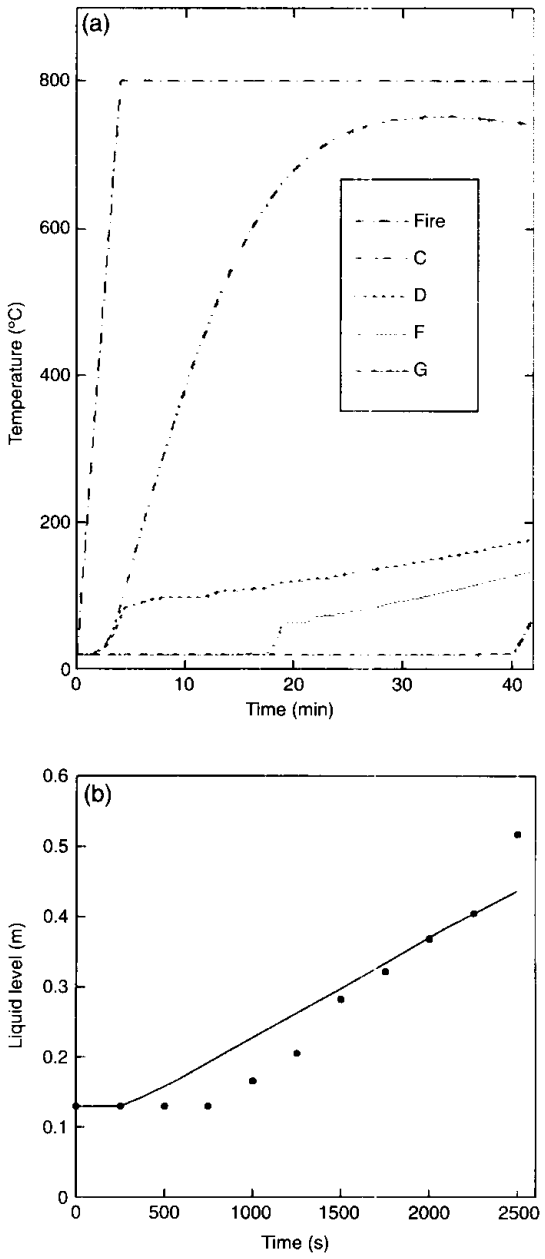

Figure 9. (a) FEM simulation of the 48Y container behaviour in a fire[15]. Temperature evolution. (○) Duret *et al*[15], (——) present results. (b) FEM simulation of the 48Y container behaviour in a fire[15]. UF_6 level evolution.

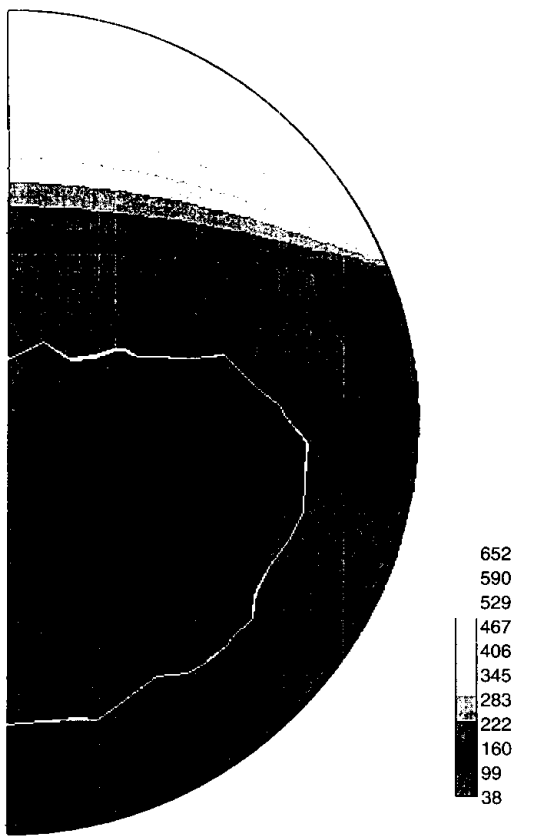

Figure 10. FEM results. Temperature distribution in a 48Y container. Simulation of the results of Reference 16, Time = 900 s. Solid boundary shown as the 64°C isotherm.

serves to supply the latent heat of liquefaction (H_{FS}). The heat transfer area is computed taking into account that its initial value is: $S_{UF6}/S = V_{UF6}/V_{CONT}$, where V_{CONT} is the container volume and $S = \pi R^2$.

The height of the UF_6 in the container is calculated from (see Figure 1):

$$H_{UF6} = R_U\,(1 + \cos(\pi - \alpha))$$

where the angle α is given by

$$\alpha + \cos\alpha \,.\, \sin\alpha = \pi \left(\frac{S_{UF6}}{S}\right)$$

and

$$S_{UF6} = \left(\frac{M_{UL}}{\rho_{UL}(t)} + \frac{M_{US}}{\rho_{US}}\right)/L$$

The fraction of wetted perimeter to the total area is:

$$S_{WET} = \alpha/\pi$$

This area fraction is used to compute the heat transfer area, since at this level the vapour is considered adiabatic.

Results

The expressions above have been applied to simulate the behaviour of an experimental container, tested in laboratory conditions. Reference 3 specifies the geometry of the container and the test conditions. Two cases will be considered, namely cases 2.4 (with T_E = 200°C of 'fire' temperature) and case 4.1 (with T_E = 400°C). They will be referred as cases 2.4 and 4.1 from hereon.

From Figure 4 in Reference 3, the time evolution of T_E, some particular times and values for T_U, T_C and the internal pressure have been retrieved. To perform the simulations, the values of the input parameters were as follows:

R_U = 0.135 m
L = 1.0 m
e = 0.03 m
λ_{US} = 9.0;
λ_{UL} = 50.0 for case 2.4;
40.0 for case 4.1;
100.0 while at triple point, case 2.4

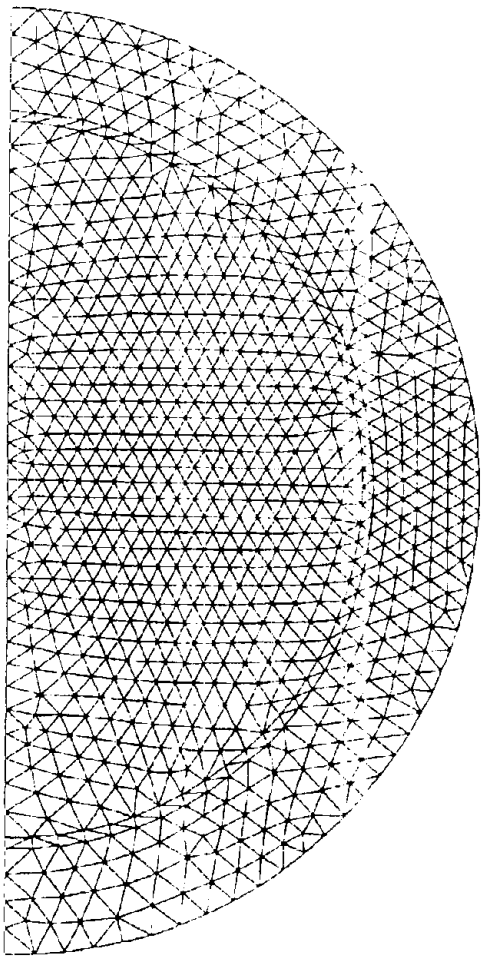

Figure 11. FEM grid used in the simulation of the experiment in Reference 3.

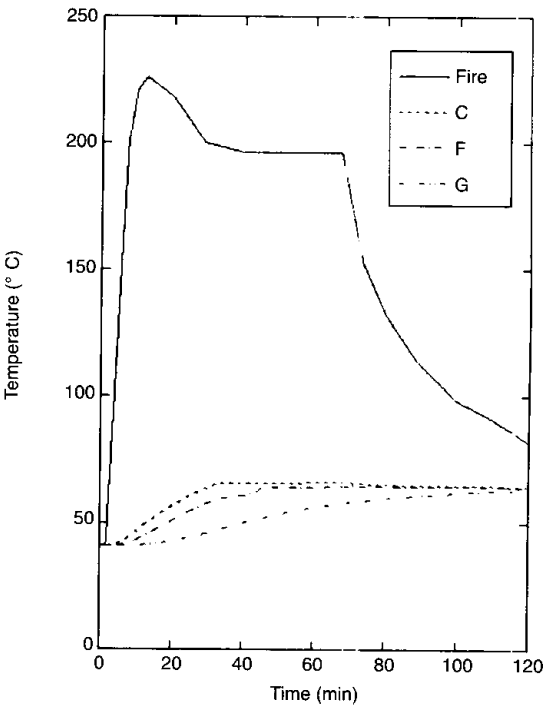

Figure 12. JCRP-10[3] FEM Simulation of Test case 2.4 (200°C). Temperature evolution.

200.0 while at triple point, case 4.1, all in $W.mK^{-1}$

λ_C = 43 $W.mK^{-1}$
ρ_{US} = 5000 $kg.m^3$
ρ_{UL} = calculated from tables, approximately 0.75 ρ_{US}
M_U = 110 kg
$M_U C_{UL}$ = 5.00×10^4
$M_U C_{US}$ = 7.93×10^4
$M_C C_C$ = 1.18×10^5
H_{FS} = 54167 $W.s.kg^{-1}$

Figure 3 shows the computed results for case 2.4. The solutions of the equations show the same trend as the experiments. In the case of experiment 4.1, the numerical results (see Figure 4) show similar behaviour. It is worth noting that the values of the effective conductivities were changed, as well as the heat transfer coefficient. In both figures, the experimental curves corresponding to the inner steel temperature and one in the UF_6 have been represented. The numerical simulation shows that the drop in the steel temperature when the UF_6 melts is adequately reflected. The values of internal pressure, computed under equilibrium hypotheses using the correlations given in Reference 4, are shown in these figures. It may be observed that the maximum value is correctly attained. However, the simulated time for this occurrence is delayed. This is due to the departure of system pressure from the equilibrium condition, a fact that is mentioned in Reference 3. Figure 5 shows a simulation of a case considering constant fire temperature to allow complete filling of the container. In this figure, the experimental values corresponding to case 4.1 are shown only for reference. The results show, in passing, how tight are the limits of heating in this experiment.

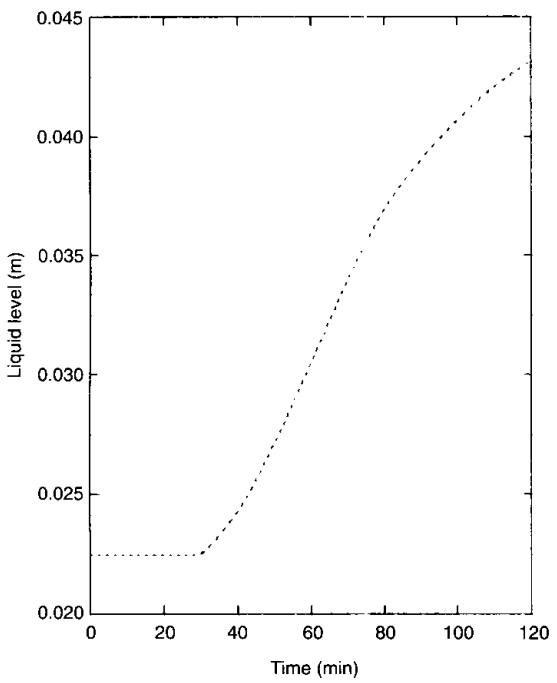

Figure 13. JCRP-10[3] FEM Simulation of Test case 2.4 (200°C). UF_6 Level evolution.

A COUPLED HEAT CONDUCTION MODEL

In this section, a coupled, distributed heat conduction model is used to simulate the behaviour of the UF_6 container[5]. Spatial variations of temperature are treated by assuming parabolic profiles with time dependent coefficients.

Heat conduction in the steel cylinder

Axial gradients will be neglected in what follows, and therefore the Fourier equation in cylindrical coordinates is written as:

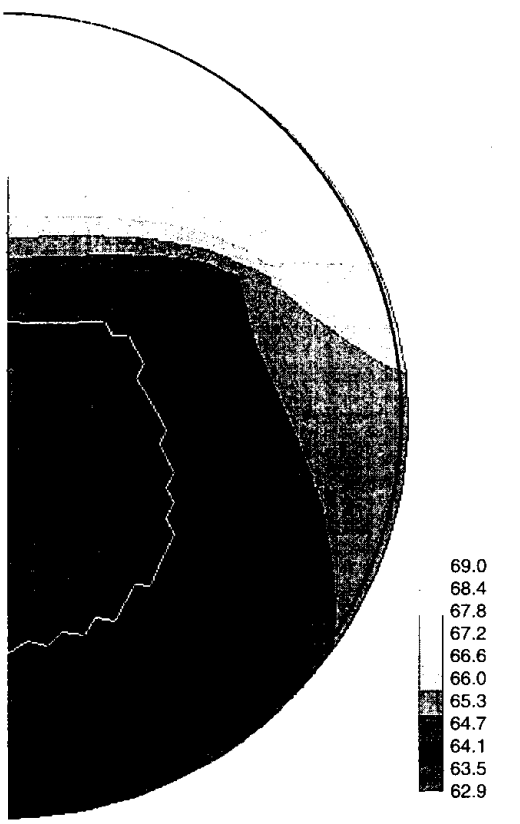

Figure 14. FEM results. Temperature distribution in the container. Simulation of the results of Reference 3, Time = 120 min. Solid boundary shown as the 64°C isotherm.

$$\frac{\partial T}{\partial t} = \frac{\alpha_c}{r}\frac{\partial}{\partial r}\left(r\frac{\partial T}{\partial r}\right) \quad (1)$$

Integrating Equation 1 between the internal and external vessel walls yields:

$$\frac{d}{dt}\int_{R_i}^{R_e} Trdr = \alpha_c r \frac{\partial T}{\partial r}\Big|_{R_i}^{R_e} \quad (2)$$

In Equation 2 the notation was changed by convenience: now $R_I = R_U$ and $R_e = R_U + e$. Let us assume a time dependent parabolic radial profile according to:

$$T = c(t)r^2 + d(t)r + e(t) \quad (3)$$

Combining Equations 2 and 3 leads to

$$\frac{d\varphi}{dt} = \alpha_c\,[2c(R_e^2 - R_i^2) + d(R_e - R_i)] \quad (4)$$

where

$$\varphi = \frac{c}{4}(R_e^4 - R_i^4) + \frac{d}{3}(R_e^3 - R_i^3) + \frac{e}{2}(R_e^2 - R_i^2) \quad (5)$$

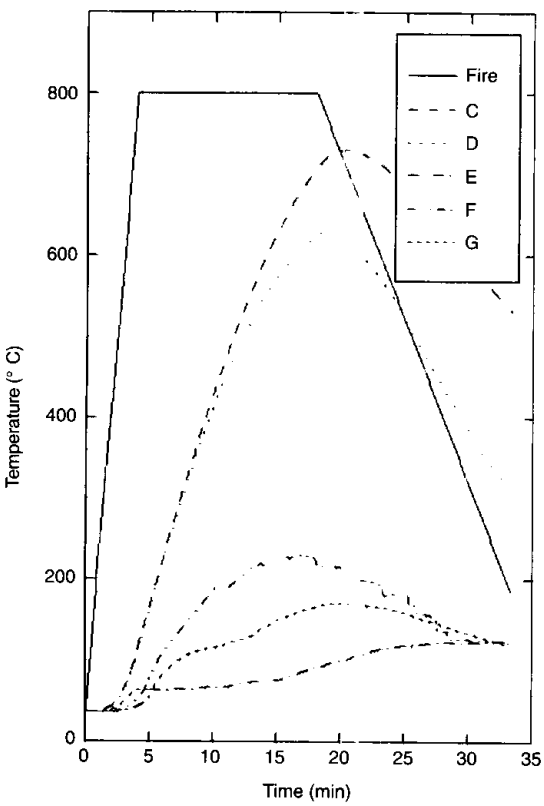

Figure 15. FEM simulation of the TENERIFE 2 experiment[17]. Temperature evolution at selected points.

The boundary condition at the external wall is given by:

$$-\lambda_C \frac{\partial T}{\partial r} = h_c\,(T - T_e) \quad (6)$$

Combining Equations 3 and 6 yields

$$(h_e R_e^2 + 2\lambda_C R_e)c + (h_e R_e + \lambda_C)d + h_e e = h_e T_e \quad (7)$$

Solid UF_6 below the triple point

Let us assume a simplified model of UF_6 as a coaxial cylinder. It is of course not exact since the UF_6 does not occupy all the inner space, but it is reasonable to expect better results than a homogeneous lumped solution. Integrating the Fourier equation in the UF_6 volume gives:

$$\frac{d}{dt}\int_0^{R_i} Trdr = \alpha_U r \frac{\partial T}{\partial r}\Big|_{R_i} \quad (8)$$

Due to radial symmetry an approximated temperature profile is written as

$$T = a(t)r^2 + b(t) \quad (9)$$

Combining Equations 8 and 9 yields

$$\frac{d\gamma}{dt} = 2R_i^2 a\alpha_U \quad (10)$$

where

$$\gamma = \frac{aR_i^4}{4} + \frac{bR_i^2}{2} \quad (11)$$

Assuming temperature and flux continuity at the inner wall leads to the boundary conditions

$$2\lambda_U R_i a - 2\lambda_C R_i c - \lambda_C d = 0 \quad (12)$$

$$aR_i^2 + b = cR_i^2 + dR_i + e \quad (13)$$

UF_6 melting

The model of melting is a UF_6 cylinder with variable radius. Care should be taken while performing the integration of the Fourier equation due to the variable upper limit. Using the Leibnitz rule, the time derivative can be extracted from the integral yielding

$$\int_0^{R_U(t)} \frac{\partial T}{\partial t} rdr = \frac{1}{2}\frac{d}{dt}\int_0^{R_U^2(t)} Tdr^2 - \frac{T_{Trip}}{2}\frac{dR_U^2}{dt} \quad (14)$$

In Equation 14, the melting boundary, $R_U(t)$, was assumed to remain at the triple point temperature, T_{Trip}. Combining Equations 9 and 14, gives

$$\frac{d\psi}{dt} = 2a\alpha_U R_U^2 \quad (15)$$

where

Table 4. Physical data for the simulation, case 3.

Material	T_{Trip}	C_S	C_L (C_G)	ρ_S	ρ_L (ρ_G)	λ_S	λ_L (λ_G)	H_{FS}
Steel	—	460.5	—	7850	—	43.0	—	—
UF_6	64.0	500.0	545.0	4950	3600	1.2	50.0	$2.8\ 10^8$
Gases	—	—	400.0	—	16.0	—	3.59	—

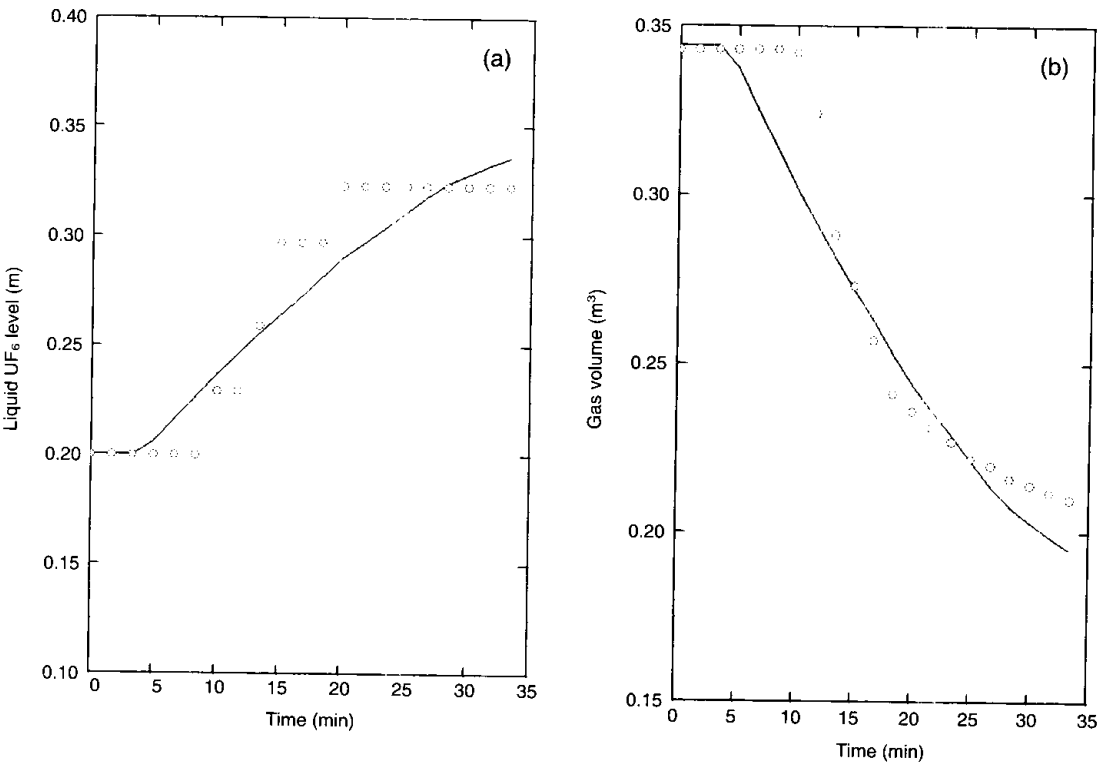

Figure 16. (a) FEM simulation of the TENERIFE 2 experiment[17]. UF_6 level evolution. (——) present work. (○) Reference 17. (b) FEM simulation of the TENERIFE 2 experiment[17]. Gas volume evolution.

Table 5. Some selected points in the container, case 3.

Point	X	Y
C	0.0	−0.135
D	0.0	−0.105
E	0.0	−0.102
F	0.0	−0.094
G	0.0	0.000

Table 6. Some selected points in the container, case 4.

Point	X	Y
C	0.0000	0.6255
D	0.4883	0.3909
E	0.4220	0.2061
F	0.0000	0.3615
G	0.0000	−0.6075

$$\psi = -\frac{aR_U^4}{4} \tag{16}$$

The flux condition at the melting boundary gives

$$2\pi R_U \left(-\lambda_U \left.\frac{\partial T}{\partial r}\right|_{R_U} + H_{FS}\rho_{US}\frac{dR_U}{dt}\right) = -\lambda_C P_W \left.\frac{\partial T}{\partial r}\right|_{R_i} \tag{17}$$

where P_W is the wetted perimeter. Combination of Equations 9 and 17 leads to

$$H_{FS}\rho_{US}\frac{dR_U}{dt} = 2a\lambda_U R_U - \frac{\lambda_C P_W}{2\pi R_U}(2cR_i + d) \tag{18}$$

The temperature condition at R_U is

$$aR_U^2 + b = T_{Trip} \tag{19}$$

Liquid–vapour UF_6 mixture

Once all the solid UF_6 has been melted, the liquid–vapour mixture increases its temperature following the Claussius-Clapeyron equilibrium curve. The model of this heat-up stage considers a uniform temperature distribution in the mixture. Therefore, the energy balance is written as

$$M_U C_U \frac{dT_U}{dt} = \lambda_C S_W(2R_i c + d) \tag{20}$$

The boundary condition at the inner wall is given by

$$cR_i^2 + dR_i + e = T_U \tag{21}$$

Results

Equations 4, 10, 15, 18 and 20 were solved using a standard package of numerical subroutines. Once again, the two cases, described in Reference 3, corresponding to the experimental test JCRP-10, were analysed: (a) case 2.4 (60 min at 200°C) and (c) case 4.1 (10 min at 400°C).

Figure 6 shows the temperature evolution in case 2.4, as obtained with the model presented in this section. The external heat transfer coefficient was adjusted to 9 $W.K^{-1}.m^{-2}$ so as to reproduce the time when melting is reached at 3 mm from the inner wall (corresponding to the thermocouple T3). Figure 7 shows the corresponding results for case 4.1. In these simulations, the apparent steel conductivity was set to 10 $W.K^{-1}.m^{-1}$. The post-solid process heat transfer coefficients were 30 and 40 $W.K^{-1}.m^{-2}$, respectively. It is important to point out that, with the exception of this, all the parameters were the same in both simulations. A shortcoming in this model is that it does not allow different temperatures during the liquefaction process. Removing this hypothesis and adding a vapour volume would improve the results.

Table 7. Some selected points in the container.

Point	X	Y
H1	0.0000	0.6255
H2	0.0000	−0.6255
H3	0.0000	−0.6095
H4	0.5683	0.2612

A FINITE ELEMENT MODEL

In this section, the generalisation of a method originally developed by Nochetto *et al*[11-14] for heterogeneous materials is presented. The technique has been validated and fully detailed in References 6–10. In this model, the relevant features of the UF_6 melting in a container are taken into account. A two-dimensional geometry is considered and the ullage is initially filled with air and, during the thermal transient, it is filled with a mixture of UF_6 and air. Symmetry with respect to the y-axis is postulated and the computational domain is discretised using triangular finite elements.

The code uses the finite-elements technique with linear interpolating basis functions. The solution is

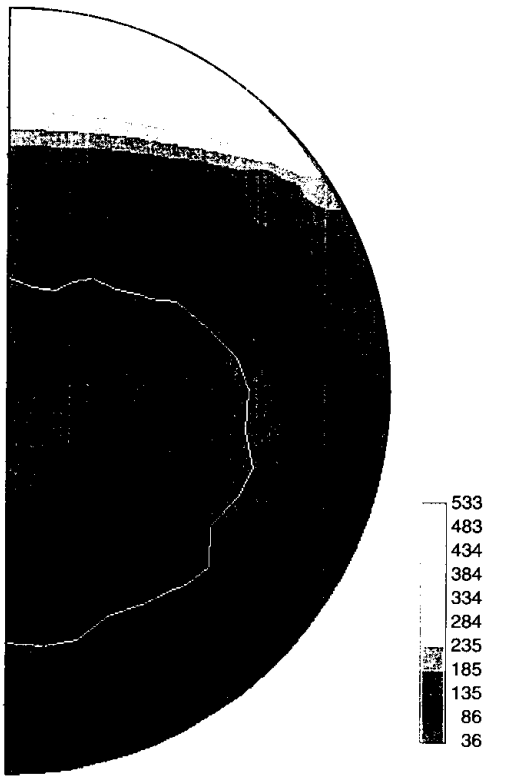

Figure 17. FEM results. Temperature distribution in a 48Y container. Simulation of the results of Reference 17, Time = 2000 s. Solid boundary shown as the 64°C isotherm.

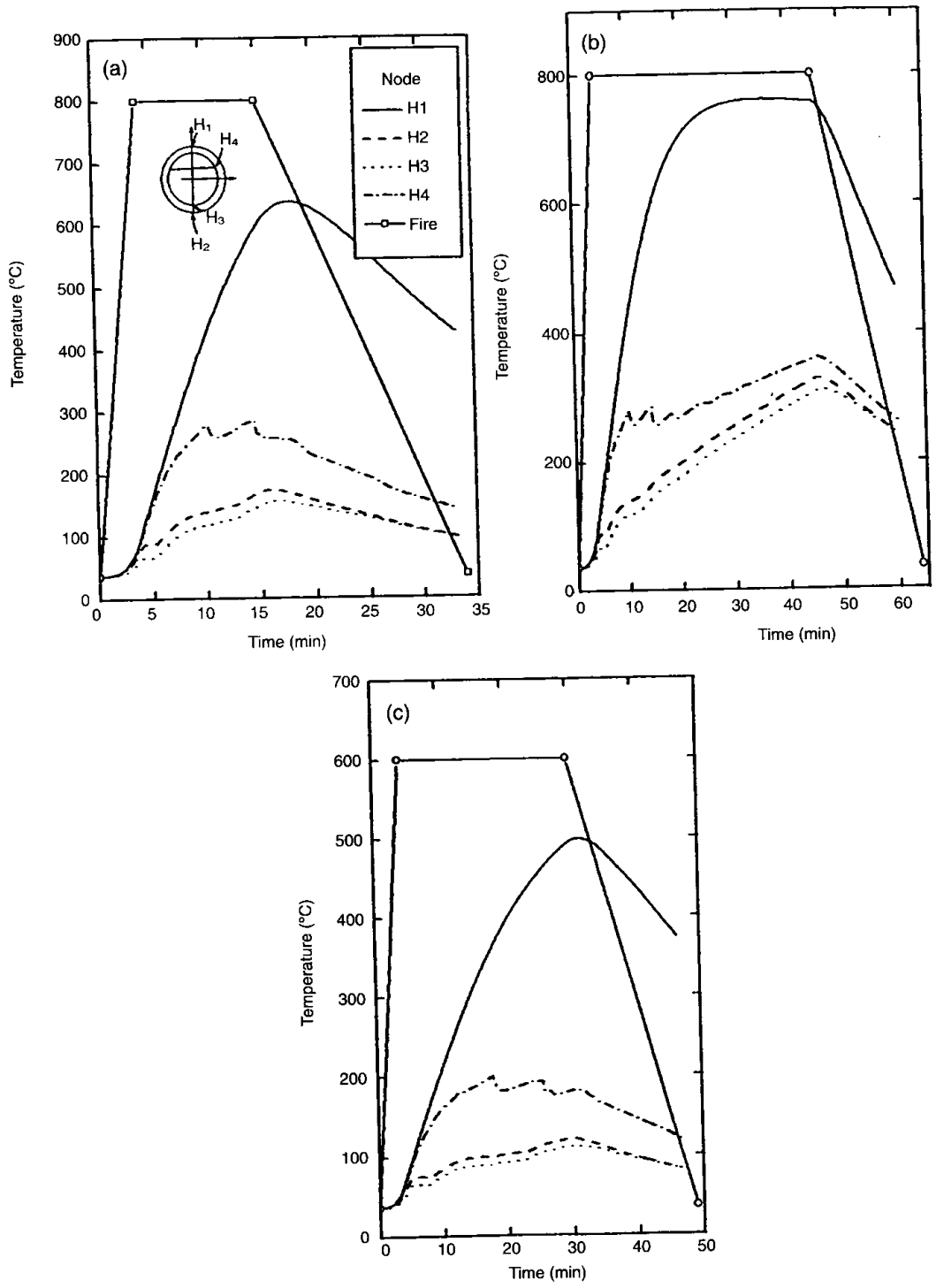

Figure 18. (a) FEM simulation of 48Y container behaviour in a fire. Fire conditions: 9 min at 800°C. Temperature evolution at selected points. Key and insert refer to (b) and (c) also. (b) FEM simulation of 48Y container behaviour in a fire. Fire conditions: 41 min at 800°C. Temperature evolution at selected points. (c) FEM simulation of 48Y container behaviour in a fire. Fire conditions: 26 min at 800°C. Temperature evolution at selected points.

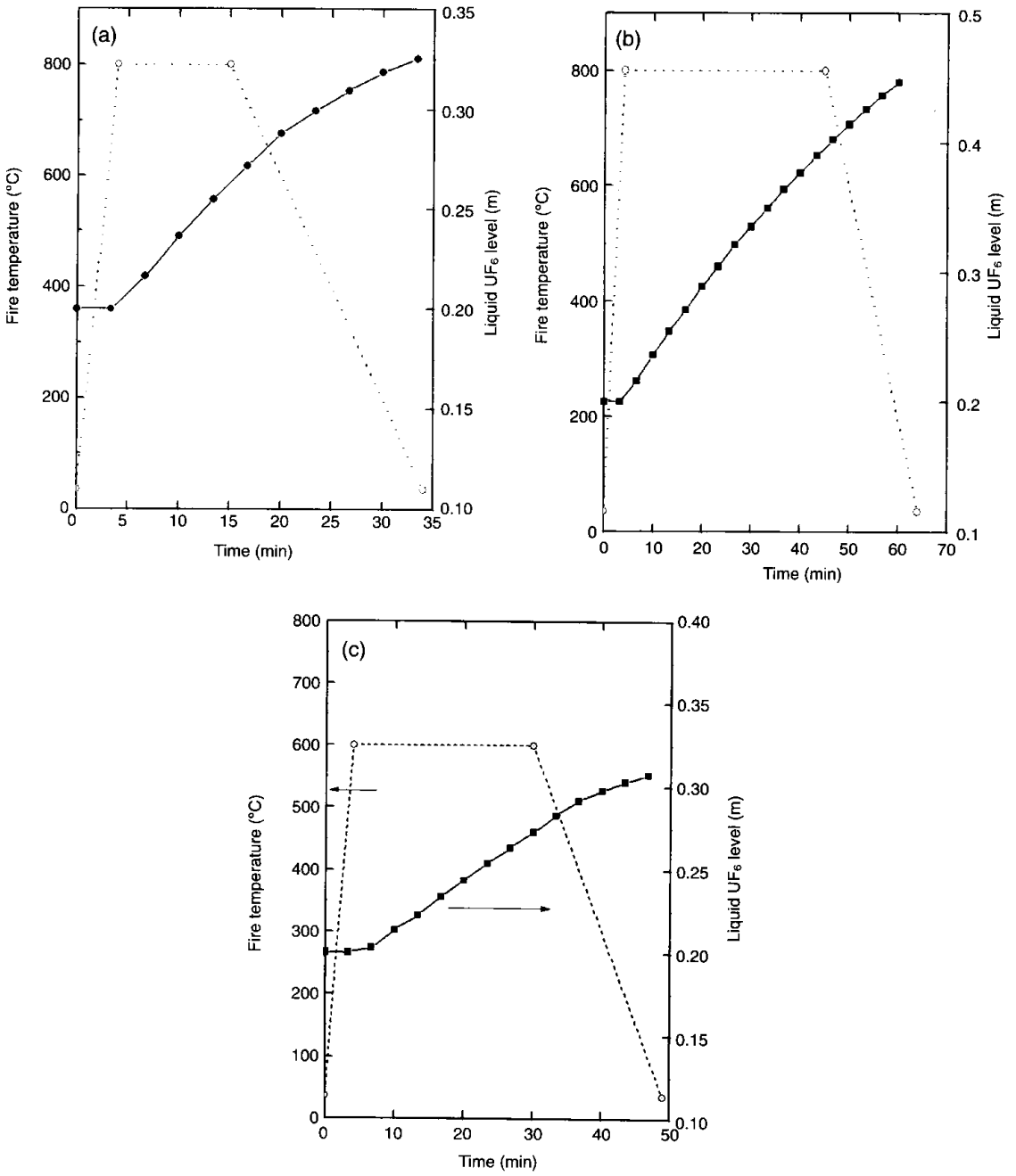

Figure 19. (a) FEM simulation of 48Y container behaviour in a fire. Fire condition: 9 min at 800°C. Time variation of UF_6 level. (b) FEM simulation of 48Y container behaviour in a fire. Fire condition: 41 min at 800°C. Time variation of UF_6 level. (c) FEM simulation of 48Y container behaviour in a fire. Fire condition: 26 min at 600°C. Time variation of UF_6 level.

computed imposing a radiation boundary condition at the external surface, according to the Stefan-Boltzmann law. When the external temperature rises, the UF_6 melts. Then, the liquid level rises, progressively filling the ullage. The relative variation of the liquid volume is computed at the end of a time step, considering the average enthalpy of each finite element. When an element is flooded, its enthalpy is assigned the latent heat of fusion and a temperature coincident with T_{Trip}. The code does not consider the 'sinking' of the non-melted UF_6 core, as due to its greater density. The relative importance of this fact does not seem to justify the use of adaptive techniques to perform the necessary grid rezoning.

Results

Case 1

The first example is a comparison with the results of Reference 15. The geometry corresponds to a 48Y container. The origin of coordinates is located at the centre of the container. The inner radius of the steel container is 0.6095 m and the external radius is 0.6255 m. The physical parameters for this run are summarised in Table 1. In this table, the sub-indexes S, L and G mean material properties evaluated for solid, fluid or vapour (gas) states, respectively. Following Reference 16 and according to common practice, the thermal conductivity of liquid UF_6 has been multiplied by 100, to get a crude approximation of the heat transfer enhancement due to natural convection. The physical parameters for the external, thermal radiation boundary conditions[15] are given in Table 2, where σ is the Boltzmann constant, ϵ is the steel emissivity and α is the steel absortivity. The environment temperature was linearly increased from 20°C to 800°C in 240 s, this temperature was kept constant up to 2500 s, when the calculation was stopped. The initial temperature of the system is 20°C.

At zero time, the UF_6 height is 0.13 m above the centre of coordinates. The grid consisted of 1191 trinodal finite elements and 642 nodes and is shown in Figure 8. Figure 9(a) shows the time variation of the temperature at selected points in the integration domain, as shown in Table 3. Points C and D are the opposite poles of the cask surface. Points D, E, F correspond to internal positions in the UF_6. The variation of temperatures is rather smooth, as expected, showing plateaus corresponding to the melting front.

Figure 9(b) shows the comparison of liquid level as computed with the present model with the values of Reference 15, shown as circles. The comparison is reasonable, given the differences between both models.

Case 2

The second example is similar to the previous one. The differences are: the variation of the environment temperature, set at 800°C from the beginning, the initial system temperature (38°C) and the initial filling height (0.1037 m). Figure 10 shows the isotherms at time t = 900 s. The isotherm corresponding to 64°C includes the solid UF_6 core and has not been smoothed. The lack of regularity is due to the method. The size and shape of the core compares well with the results of Reference 16. This is encouraging, given the differences in the modelling. The simulation was run up to 2600 s, this allowed for the complete melting of the solid core. This, in turn, allows verifying the code, because the final height may be calculated algebraically. In this case, this value is 0.4348 m. The calculated value was 0.42 m. The agreement is reasonable, given the approximate way in which the change of volume is obtained in the code. The height of the liquid in the container agrees very well with the curve quoted in Reference 16 up to t = 900 s. After this time the agreement disappears. However, the final value shown in Reference 16 is not correct.

Case 3

The third example consists in the simulation of the results of Reference 3, as done with the simplified models of the first and second Sections. The initial height is 0.02245 m. Figure 11 shows the finite element grid used, consisting of 1732 elements and 912 nodes. The physical parameters adopted are listed in Table 4. The emissivity was 0.6, as in Reference 3, Table 2. Figure 12 shows the variation of temperature at selected points in the system up to 1200 s. Point coordinates are shown in Table 5.

Figure 13 shows the time variation of liquid level, while Figure 14 shows the isotherms for t = 7200 s. Sensitivity analyses to test the effect of the liquid conductivity and to different grid nodalisation did not show significant differences.

Case 4

Case 4 corresponds to the simulation of the TENERIFE 2 experiment[17]. The cask is a 48Y container. The initial temperature is 36°C and the initial UF_6 height is 0.2 m. The environment temperature rises linearly from 36°C to 800°C in 240 s. It is kept constant up to time t = 1080 s and then decreased linearly to 36°C at time t = 2200 s. Figure 15, curve B, shows this variation. The grid used is the same as in case 1. The physical parameters are those of Table 4, with the exception of λ_S, now taken as 3.6. Figure 15 shows the time variation of temperature at the points whose coordinates are shown in Table 6.

Points C and D are located on the external face of the cask. Points E and G are located in the UF_6 mass and Point F is located in the vapour zone. These points

correspond with the location of the thermocouples in the TEN2 experience. Curves E and G show the plateaus associated with the melting front. The oscillations in curve F may be due to the flooding of the elements by melted UF_6. The comparison of present results with those of Reference 17 is not completely satisfactory. Discrepancies may originate in the difference between the models. The model of Reference 16 is quite more detailed, at the expense of one order of magnitude higher computational cost. Figures 16(a) and 16(b) show the time variation of the liquid UF_6 level and the variation of the volume of the ullage gases respectively. The correspondence between present results and those of Reference 17 is acceptable. Finally, Figure 17 shows the isotherms distribution at time t = 2000 s.

ADDITIONAL RESULTS

The finite element model was also run to consider some additional, representative cases. The geometry of the 48Y container was adopted and three fire conditions were considered. The points have been selected according to the definitions in Table 7.

Points H1 and H3 are located on the external face of the cask. Point H2 is located in the lower point of the UF_6 mass and Point H4 is located in the vapour zone, at the initial interface position. Figures 18(a–c) show the corresponding time variations of the temperatures for different duration of the fire and different maximum temperature. Figures 19(a–c) show the corresponding time variations of the UF_6 liquid levels for the same conditions. Finally, Figures 20(a–c) show the corresponding maps of temperature distribution.

CONCLUSIONS

A series of increasingly complex models have been developed, aimed at predicting the behaviour of UF_6 containers in fires. The models provided valuable information, according to their resolution. Simple models provide an economical technique, but the results have shown case-by-case dependence. The FEM model has a broader scope. However, due to assumptions related to no natural circulation in the fluid and no solid sinking, the results of the FEM model are not much more accurate than those obtained from the simplified models. It is the authors' opinion that the FEM code or a lumped-parameter approximation, both dealing with the non-equilibrium aspects of the problem should give reasonable results, that may be used to perform safety-related calculations. At present, results may be considered satisfactory enough. This was the main task of our effort and, consequently, it has been accomplished.

ACKNOWLEDGEMENTS

The authors gratefully acknowledge the IAEA for its support through CRA 7285 during the course of the project. They also acknowledge the comments of the referees, which improved the presentation of the paper.

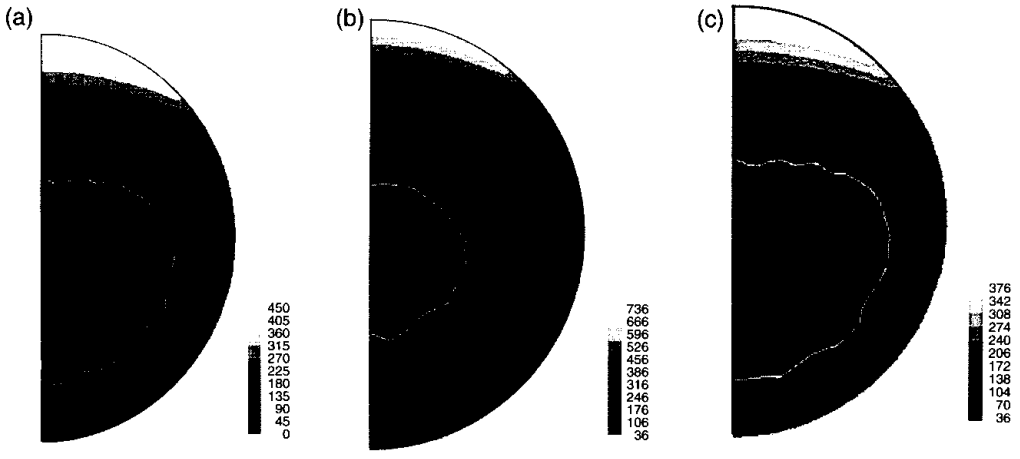

Figure 20. (a) FEM results. Map of isotherms in a 48Y container. Fire conditions: 9 min at 800°C. Time = 2000 s. Solid boundary shown as the 64°C isotherm. (b) FEM results. Map of isotherms in a 48Y container. Fire conditions: 41 min at 800°C. Time = 3000 s. Solid boundary shown as the 64°C isotherm. (c) FEM results. Map of isotherms in a 48Y container. Fire conditions: 26 min at 600°C. Time = 2800 s. Solid boundary shown as the 64°C isotherm.

REFERENCES

1. Ferreri, J. C. and Clausse, A. *Computational Models for the Simulation of the Behavior of UF_6 in Fires.* In: Proc. IAEA Technical Committee Meeting on the Safety of UF_6 Containers in Fires, Oak Ridge, USA, October 1994.

2. Clausse, A. and Ferreri, J. C. *Comportamiento termodinámico de un contenedor de UF_6 sometido a altas temperaturas.* (In Spanish) CNEA Internal Memorandum (1993).
3. Hasegawa, M., Tanaka, T., Takahashi, M., Yato, Y. and Sasao, N. *Thermal Analysis on a 48Y Type UF_6 Package* (Power Reactor and Nuclear Fuel Development Corporation) Rep. JCRP-10 (1990). These results are also reported by Suzuki, M., Ohkuma, Y., Ikou, S., Shimizu, K., Akiyama, T. and Yato, Y. in *An Experimental Study on Heat Transfer of a UF_6-filled vessel.* In: Proc. Conf. on Uranium Hexafluoride: Safe handling, Processing and Transporting, Oak Ridge, Tennessee, 24–26 May 1988.
4. Anderson, J. C., Kerr, C. P. and Williams, W. R. *Correlation of the Thermophysical Properties of Uranium Hexafluoride Over a Wide Range of Temperature and Pressure* (Oak ridge National Laboratory, U.S.A.) ORNL/ENG/TM-51 (1994).
5. Clausse, A. and Ferreri, J. C. *A Model of Melting of Stored UF_6 Subject to High Temperatures.* CNEA Internal Memorandum (1995).
6. Basombrío, F. G. *FASES: Un Programa para resolver el Problema de Stefan basado en Elementos Finitos* (in Spanish), Informe Técnico CNEA-CAB 35/01/95 (CNEA, Agosto) (1995).
7. Basombrío, F. G. *Resolución Numérica del Problema de Stefan para Materiales Heterogéneos* (in Spanish), Internal Publication Series, National Board of Nuclear Regulation (Argentina), ENREN PI-4/96 (1996).
8. Basombrío, F. G. *El Problema de Stefan de dos Fases en Materiales Heterogéneos. Aplicaciones* (in Spanish), Revista Internacional de Métodos Numéricos en Ingeniería **13**, 351–366 (1997).
9. Basombrío, F. G. *Modelado por Elementos Finitos de Situaciones de Incendio en Contenedores para el Transporte de UF_6* (in Spanish), Internal Publication Series, National Board of Nuclear Regulation (Argentina), ENREN PI-12/96 (1996).
10. Basombrío, F. G. *The Two-phase Problem in Heterogeneous Materials.* In: Proc. of IV World Congress in Computational Mechanics, Buenos Aires, Argentina, 29 June–2 July 1998.
11. Nochetto, R. H. and Verdi, C. *Approximation of Degenerate Parabolic Problems Using Numerical Integration.* S.I.A.M. J. Numerical Anal. **25**, 784–814 (1988).
12. Nochetto, R. H. *Finite Element methods for Parabolic Free Boundary Problems.* In: Advances in Numerical Analysis, W. Light (Ed.), Vol. 1, Ch. 2, pp. 34–95 (Oxford Univ. Press) (1991).
13. Nochetto, R. H., Paolini, M. and Verdi, C. *An Adaptive Finite Element Method for Two-phase Stefan Problems in Two-space Dimensions. Part I: Stability and Errors Estimates.* Math Comput **57**, 73–108 (1991).
14. Nochetto, R. H., Paolini, M. and Verdi, C. *An Adaptive Finite Element Method for Two-phase Stefan Problems in Two-space Dimensions. Part II: Implementation and Numerical Experiments.* S.I.A.M. J. Sci. Stat. Comput. **12**, 1207–1244 (1991).
15. Duret, B. *Thermo-Mechanical Modeling of a UF_6 Container in a Fire.* Report STI/LASP/93 30/BD (Commisarial de l'Energié Atomique, Centre d'Etudes de Grenoble, France) (October 1993).
16. Lewis, R. W., Zheng, Y. and Ghetin, D. T. *An Adaptive Finite Element Model for the Behavior of Uranium Hexafluoride filled Container in a Fire.* Nucl. Eng. Des. **140**, 229–250 (1993).
17. Anon. *Modeling of a UF_6 Container in a Fire.* Report CEA/DTP/95 EP (Commisariat de l'Energié Atomique, Centre d'Etudes de Grenoble, France) (1995).